

Polarized semi-inclusive deep-inelastic scattering at NNLO in QCD

Leonardo Bonino, Thomas Gehrmann, Markus Löchner, and Kay Schönwald
Physik-Institut, Universität Zürich, Winterthurerstrasse 190, 8057 Zürich, Switzerland

Giovanni Stagnitto
Università degli Studi di Milano-Bicocca & INFN, Piazza della Scienza 3, 20216 Milano, Italy

Semi-inclusive hadron production in longitudinally polarized deep-inelastic lepton-nucleon scattering is a powerful tool for resolving the quark flavor decomposition of the proton's spin structure. We present the full next-to-next-to-leading order (NNLO) QCD corrections to the coefficient functions of polarized semi-inclusive deep-inelastic scattering (SIDIS) in analytical form, enabling the use of SIDIS measurements in precision studies of the proton spin structure. The numerical impact of these corrections is illustrated by a comparison with data of polarized single-inclusive hadron spectra from the DESY HERMES and CERN COMPASS experiments.

INTRODUCTION

The proton is a complex bound state of quarks and gluons. Its internal structure can be described in a probabilistic manner in the parton model, formulated in the framework of the theory of strong interactions (quantum chromodynamics, QCD). Owing to a large wealth of experimental data from hadron colliders and lepton-hadron scattering, the momentum distributions of quarks and gluons (parton distribution functions, PDFs) are now known to per-cent level accuracy [1–4].

The understanding of other aspects of the proton structure is much less well-developed. Most notably, information on the proton's spin structure [5] is still quite sparse, relying on a limited set of data from polarized lepton-nucleon scattering at fixed target energies and from polarized proton-proton collisions at the BNL RHIC collider. It is one of the primary objectives of the planned electron-ion collider (EIC) at BNL to provide in-depth probes of the nucleon spin structure through a variety of different measurements in polarized electron-proton collisions [6].

An essential aspect of the proton's spin structure is encoded in polarization-dependent PDFs, describing the probability of finding a parton with a given momentum fraction x at a resolution scale Q^2 with its helicity aligned or anti-aligned to the nucleon's spin. One considers the unpolarized and polarized combinations:

$$\begin{aligned} f(x, Q^2) &= f^+(x, Q^2) + f^-(x, Q^2), \\ \Delta f(x, Q^2) &= f^+(x, Q^2) - f^-(x, Q^2), \end{aligned} \quad (1)$$

where \pm refers to the relative orientation of the parton helicity with respect to the parent nucleon spin. $f(x, Q^2)$ are the well-established (unpolarized) PDFs, while $\Delta f(x, Q^2)$ contain the essential information on the spin structure of the nucleon. Experimental probes of the polarized PDFs $\Delta f(x, Q^2)$ rely on the measurement of asymmetries in collisions where both probe and target are longitudinally polarized.

The main experimental information entering into the

determination of polarized PDFs [7, 8] comes from polarized deeply inelastic lepton-nucleon scattering [9–16], which probes specific charge-weighted combinations of the polarized quark distributions. Semi-inclusive identified hadron production in deep inelastic scattering (SIDIS) offers valuable supplementary information [17–19], since the identified hadron species can be associated to the flavor of the parton that was produced in the underlying hard scattering process. This connection is described by fragmentation functions (FFs), encoding the probability of a parton fragmenting into a hadron of a given type. Similar to the PDFs, FFs are universal, non-perturbative objects that factorize from the parton-level subprocess and whose evolution with the resolution scale is determined by the DGLAP equations. Especially future SIDIS measurements at the BNL EIC will provide an indispensable tool to disentangle the precise flavor structure of the nucleon spin [20, 21].

Global fits of the unpolarized PDFs are routinely performed at next-to-leading order (NLO) and next-to-next-to-leading order (NNLO) in QCD, thereby requiring corrections at the appropriate order to the evolution kernels and to the parton-level cross sections for all experimental observables that are included in the fits.

For polarized PDFs, the evolution kernels are known to NLO [22, 23] and NNLO [24–26], but corrections to parton-level coefficient functions beyond NLO have up to now been obtained only for inclusive polarized DIS [27, 28]. The polarized SIDIS coefficient functions are currently known to NLO [29]. Following up on initial leading-order (LO) studies [30, 31], polarized PDFs have been determined routinely at NLO though global fits [7, 8, 32–37] to spin-asymmetry data.

In view of future precision data from the BNL EIC, an extension of polarized PDF studies to NNLO accuracy would be very much desirable. With the enhanced precision and including polarized SIDIS measurements, these will not only help disentangle the PDFs of polarized gluons, valence and sea quarks, but also allow to discern quark and anti-quark contributions to the polar-

ized flavor PDFs. First steps in this direction were taken most recently, with an NNLO fit [38] to polarized inclusive DIS and SIDIS data, approximating [39] the NNLO SIDIS coefficient functions from a threshold expansion.

With this letter, we enable consistent precision studies by computing the NNLO QCD coefficient functions for longitudinally polarized SIDIS, following up on recent NNLO results obtained for unpolarized SIDIS [40, 41].

KINEMATICS OF POLARIZED SIDIS

We consider the observation of an unpolarized hadron h from the scattering of a polarized lepton off a polarized nucleon. Both polarizations are longitudinal. Following the notation of [29, 42], we describe polarized semi-inclusive deep-inelastic scattering as $\bar{\ell}(k)\bar{p}(P) \rightarrow \ell(k')h(P_h)X$, with some inclusive final-state radiation X . The vector $q = k - k'$ denotes the momentum transfer between the leptonic and hadronic systems, and $y = (P \cdot q)/(P \cdot k)$ the associated energy transfer at virtuality $Q^2 = -q^2$. The quantities

$$x = \frac{Q^2}{2P \cdot q} \quad \text{and} \quad z = \frac{P \cdot P_h}{P \cdot q} \quad (2)$$

are the momentum fractions of the nucleon carried by the incoming parton (x), and of the outgoing parton carried by the identified hadron (z) at Born level. The center-of-mass energy of the lepton-nucleon system \sqrt{s} is given by $s = Q^2/(xy)$.

The experimentally measured double spin asymmetry is obtained from the difference of anti-aligned and aligned spin orientations of probe and target [43]. After correcting for QED effects and neglecting higher-twist contributions, it can be expressed as ratio of hadronic SIDIS structure functions as

$$A_1^h(x, z, Q^2) = \frac{g_1^h(x, z, Q^2)}{F_1^h(x, z, Q^2)}. \quad (3)$$

The g_1^h polarized SIDIS structure function receives contributions from different partonic channels. These are given by the convolution between the polarized PDF Δf_p for a parton p , the FF D_p^h of parton p' into hadron h , and the polarized coefficient function $\Delta C_{p'p}$ for the partonic transition $p \rightarrow p'$:

$$2g_1^h(x, z, Q^2) = \sum_{p,p'} \int_x^1 \frac{d\hat{x}}{\hat{x}} \int_z^1 \frac{d\hat{z}}{\hat{z}} \Delta f_p \left(\frac{x}{\hat{x}}, \mu_F^2 \right) \times D_{p'}^h \left(\frac{z}{\hat{z}}, \mu_A^2 \right) \Delta C_{p'p} \left(\hat{x}, \hat{z}, Q^2, \mu_R^2, \mu_F^2, \mu_A^2 \right). \quad (4)$$

Likewise, the unpolarized SIDIS structure function F_1^h

reads

$$2F_1^h(x, z, Q^2) = \sum_{p,p'} \int_x^1 \frac{d\hat{x}}{\hat{x}} \int_z^1 \frac{d\hat{z}}{\hat{z}} f_p \left(\frac{x}{\hat{x}}, \mu_F^2 \right) \times D_{p'}^h \left(\frac{z}{\hat{z}}, \mu_A^2 \right) C_{p'p}^T \left(\hat{x}, \hat{z}, Q^2, \mu_R^2, \mu_F^2, \mu_A^2 \right). \quad (5)$$

In the above expressions, μ_F and μ_A denote the mass factorization scales of PDFs and FFs, while μ_R is the renormalization scale. The SIDIS coefficient functions $(\Delta)C_{p'p}$ encode the hard-scattering part of the process, and can be computed in perturbative QCD. Their perturbative expansion in the strong coupling constant α_s reads

$$(\Delta)C_{p'p} = (\Delta)C_{p'p}^{(0)} + \frac{\alpha_s(\mu_R^2)}{2\pi} (\Delta)C_{p'p}^{(1)} + \left(\frac{\alpha_s(\mu_R^2)}{2\pi} \right)^2 (\Delta)C_{p'p}^{(2)} + \mathcal{O}(\alpha_s^3). \quad (6)$$

At LO, only the qq channel ($\gamma^*q \rightarrow q$) contributes, with the LO coefficient function normalized to

$$\Delta C_{qq}^{(0)} = e_q^2 \delta(1-\hat{x})\delta(1-\hat{z}), \quad (7)$$

where e_q is the quark charge. At NLO [29], the channels gg and gq start to contribute, yielding $\Delta C_{qq}^{(1)}$, $\Delta C_{gq}^{(1)}$ and $\Delta C_{qg}^{(1)}$.

In this letter we present results for the NNLO corrections $\Delta C_{p'p}^{(2)}$ to all partonic channels appearing at this order. Following the notation of [41, 44], the seven partonic channels appearing at $\mathcal{O}(\alpha_s^2)$ are:

$$\begin{aligned} \Delta C_{qq}^{(2)} &= e_q^2 \Delta C_{qq}^{\text{NS}} + \left(\sum_j e_{q_j}^2 \right) \Delta C_{qq}^{\text{PS}}, \\ \Delta C_{\bar{q}q}^{(2)} &= e_q^2 \Delta C_{\bar{q}q}, \\ \Delta C_{q'q}^{(2)} &= e_q^2 \Delta C_{q'q}^1 + e_{q'}^2 \Delta C_{q'q}^2 + e_q e_{q'} \Delta C_{q'q}^3, \\ \Delta C_{\bar{q}'q}^{(2)} &= e_q^2 \Delta C_{\bar{q}'q}^1 + e_{q'}^2 \Delta C_{\bar{q}'q}^2 - e_q e_{q'} \Delta C_{\bar{q}'q}^3, \\ \Delta C_{gq}^{(2)} &= e_q^2 \Delta C_{gq}, \\ \Delta C_{qg}^{(2)} &= e_q^2 \Delta C_{qg}, \\ \Delta C_{gg}^{(2)} &= \left(\sum_j e_{q_j}^2 \right) C_{gg}. \end{aligned} \quad (8)$$

With $(\bar{q})'$ we indicate an (anti-)quark of flavor different from q .

ANALYTICAL CALCULATION

To obtain the matrix elements relevant to the polarized coefficient functions, we use the projectors from the inclusive calculation [27]. The appearance of the inherently four-dimensional objects γ_5 and $\varepsilon^{\mu\nu\rho\sigma}$ in the external projectors requires a consistent treatment in dimensional regularization [45]. A common choice is the

't Hooft-Veltman-Breitenlohner-Maison (HVBM) scheme [45, 46]. The Larin prescription [47, 48] is derived from the HVBM scheme, and consists of setting

$$\gamma_\mu \gamma_5 = \frac{i}{3!} \varepsilon_{\mu\nu\rho\sigma} \gamma^\nu \gamma^\rho \gamma^\sigma \quad (9)$$

and evaluating the Dirac traces in d dimensions. The two remaining Levi-Civita tensors are contracted into d -dimensional metric tensors. Quantities in the Larin scheme will be denoted by an upper index L, and are subsequently converted to the $\overline{\text{MS}}$ scheme.

The NNLO corrections consist of three types of contributions, defined relative to the underlying Born process: double-real (RR) corrections stem from two additional radiations, the real-virtual (RV) corrections from a one-loop correction and an additional radiation, and the double-virtual (VV) corrections from two-loop virtual insertions.

The evaluation and integration of the RR and RV contributions proceed like in the unpolarized calculation [41]: following integration-by-part (IBP) reduction [49, 50] with `Reduze2` [51], the RR contributions are expressed in terms of 21 master integrals, which were computed by solving their differential equations [52]. Their analytic expressions will be presented in [53]. The RV integrals are solved by analytically integrating out the loop [52], then continuing the appearing hypergeometric functions to the appropriate Riemann sheets and subsequently expanding out the phase space measure in terms of distributions in each of the sheets as described in [54]. The master integrals for the VV part are taken from [55].

The calculation is carried out using `Mathematica` and `FORM` [56]. We express the integrals in terms of harmonic polylogarithms (HPLs) [57] with the help of the packages `HPL` [58] and `PolyLogTools` [59].

Interestingly, the NLO virtual (V) and the NNLO VV contributions to g_1^h are described by the respective vector form factors [55] rather than by their axial counterparts: the photon couples to the quark line through a vector coupling, whereas the antisymmetric current carried by the photon is contracted only from the external leg. As a consequence, traces of quark-loops coupling to the polarized photon can be carried out consistently in $d = 4 - 2\epsilon$ dimensions without giving rise to the axial anomaly [60, 61]. This stands in sharp contrast to calculations of operator matrix elements (OME), e.g. [62], where the g_1 projector of the photon is absorbed into an operator insertion, rendering the photon coupling axial, and giving rise to the anomaly.

We renormalize α_s in the $\overline{\text{MS}}$ scheme to remove poles of ultraviolet origin. The remaining infrared poles can be eliminated by mass factorization on the polarized PDFs and unpolarized FFs. At this stage, all coefficient functions are formulated in the Larin scheme. Consequently, the polarized PDF mass factorization counterterms are

taken in the Larin scheme, constructed from the polarized spacelike splitting functions in this scheme.

These splitting functions [22, 23] in Larin and $\overline{\text{MS}}$ are related by a scheme transformation [27], which follows from the scheme invariance of the measurable inclusive structure function g_1 [62]:

$$g_1 = \Delta C^{\overline{\text{MS}}} \otimes \Delta f^{\overline{\text{MS}}} \\ = (\Delta C^{\text{L}} \otimes Z^{-1}) \otimes (Z \otimes \Delta f^{\text{L}}) = \Delta C^{\text{L}} \otimes \Delta f^{\text{L}} \quad (10)$$

with

$$\Delta C = \begin{pmatrix} \Delta C_q \\ \Delta C_g \end{pmatrix}^T, \quad \Delta f = \begin{pmatrix} \Delta q \\ \Delta g \end{pmatrix}, \quad Z = \begin{pmatrix} z_{qq} & z_{qg} \\ z_{gq} & z_{gg} \end{pmatrix}, \quad (11)$$

where the entries of Z in non-singlet and singlet case are given in [24]. All convolutions are carried out by using `MT` [63].

In order to obtain the $\overline{\text{MS}}$ SIDIS coefficient functions, we scheme-transform the Larin-scheme coefficient functions according to (10). Our results with full scale dependence (μ_R , μ_F , μ_A) are provided in an ancillary file to the `arXiv` submission of this paper.

Several checks were performed to validate our results. We verified that our results in each of the channels in (8) fulfill the renormalization group equations in both Larin and $\overline{\text{MS}}$ scheme. Moreover, we used the underlying RR, RV and VV polarized subprocess matrix elements to re-derive the inclusive NNLO coefficient function for g_1 , finding full agreement with [27]. We subsequently integrated specific subprocess contributions to the SIDIS coefficient functions over the final-state parton momentum fraction z , recovering the respective contributions to the g_1 coefficient functions. Finally, we compared our leading and subleading power terms for the $\Delta C_{qq}^{(2)}$ coefficient function against the prediction from NNLL threshold-resummation in [39], finding full agreement.

RESULTS

Measurements of SIDIS for various species of final state hadrons on proton targets were performed by CERN COMPASS [18] and the DESY HERMES [19] fixed-target experiments. The experiments present their results in terms of the longitudinal double spin asymmetry A_1^h (3). COMPASS [18] measured at $\sqrt{s} = 17.4$ GeV and included all hadrons produced in the range $0.2 < z < 0.85$. The HERMES [19] data were taken at $\sqrt{s} = 7.25$ GeV and included hadrons in the range $0.2 < z < 0.85$. The asymmetry A_1^h is evaluated at central bin values in x and Q^2 , justified by a relatively narrow range in Q^2 for each bin due to the kinematical restrictions of the experiments.

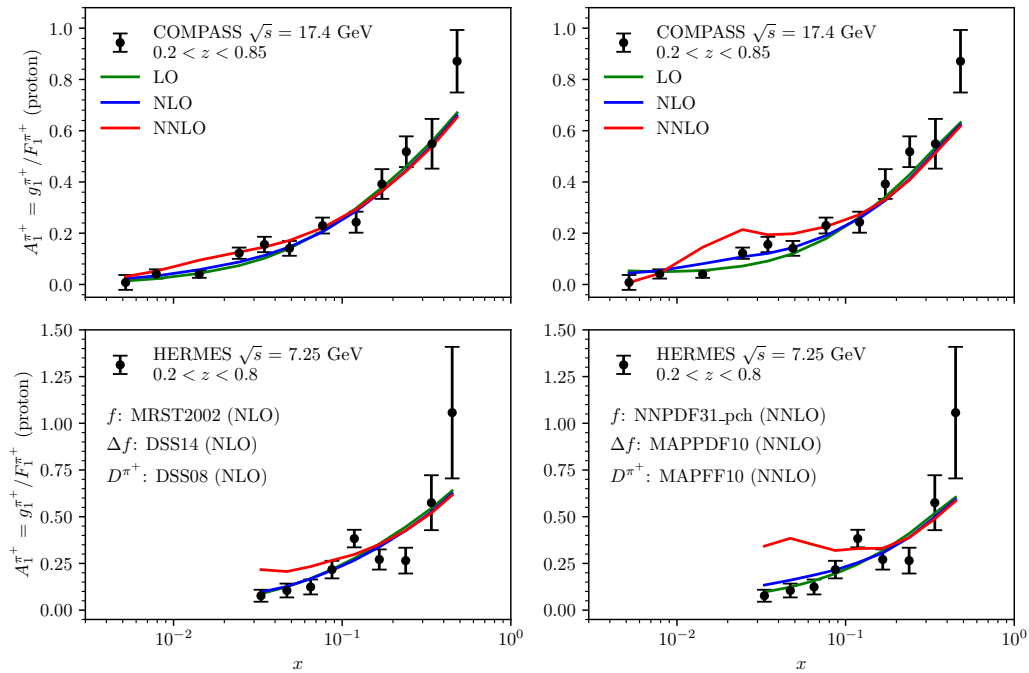


FIG. 1. Asymmetries $A_1^{\pi^+}$ at different perturbative orders compared to data from COMPASS [18] and HERMES [19], computed using NLO PDFs and FFs (left) and NNLO PDFs and FFs (right).

To illustrate the numerical impact of the newly computed NNLO corrections to the polarized SIDIS coefficient functions, we compare the predictions for $A_1^{\pi^+}$ to predictions at LO, NLO and NNLO. To single out the impact of the coefficient functions, predictions at the different orders are computed with the same sets of parton distributions and fragmentation functions. Since the only currently available NNLO polarized PDF set, the MAPPDF1.0 set [38], is not based on a global fit, we display predictions for two different setups. (A) PDFs and FFs at NLO throughout: we use the polarized NLO PDF DSSV14 set [8], in combination (as used in the original DSSV14 fit) with unpolarized NLO PDFs from the MRST2002 set [64] and NLO FFs from the DSS08 set [65]. (B) PDFs and FFs at NNLO throughout: we use the polarized NNLO MAPPDF1.0 set [38], with unpolarized PDFs from NNPDF3.1 [66] and FFs from MAPFF1.0 [67].

Figure 1 compares the predictions for $A_1^{\pi^+}$ from COMPASS [18] and HERMES [19]. We observe that the predictions for the asymmetry are very stable between LO and NLO. Including the NNLO corrections slightly decreases the asymmetry at high x and leads to a substantial enhancement of the asymmetry at lower values of x . These changes are more pronounced for the predictions using NNLO PDFs and FFs (right frames). The bumps that are observed in these predictions at NNLO can be traced back to an oscillatory behavior of the polarized gluon distribution at low Q^2 in MAPPDF1.0 [38]. This

behavior could be an artifact due to lack of constraining power of the dataset used in the MAPPDF1.0 fit on the polarized gluon distribution, which is overcome by the inclusion of hadron collider data in the DSSV14 set [8]. Both the COMPASS and HERMES datasets on $A_1^{\pi^+}$ were included in the DSSV14 and MAPPDF1.0 fits of polarized PDFs, using exact SIDIS coefficient functions at NLO and, in the case of MAPPDF1.0, an approximation [39] at NNLO. The numerical magnitude of the NNLO corrections to the SIDIS asymmetry $A_1^{\pi^+}$ at low x clearly demonstrates the potential impact of the exact corrections and calls for a careful reassessment of the impact of SIDIS data in a future global fit at NNLO.

In Figure 2 we study the impact of each partonic channel on $g_1^{\pi^+}$ at LO, NLO and NNLO for COMPASS kinematics. We use NLO PDFs and FFs throughout in order to avoid spurious effects from the polarized gluon distribution in [38]. For x and Q^2 we use the central values of the kinematical bins from the COMPASS analysis [18], integrating over $z \in [0.2, 0.85]$. While the $q \rightarrow q$ channel remains the dominant contribution, the $q \rightarrow g$ channel plays a more prominent role at NNLO than at NLO, but in the small- x region also the $g \rightarrow q$ channel provides a sizable contribution starting from NNLO. We notice a reduction in the size of the NNLO corrections for larger values of x (and in turn of Q^2), which points at an improvement in the convergence of the perturbative series with increasing Q^2 .

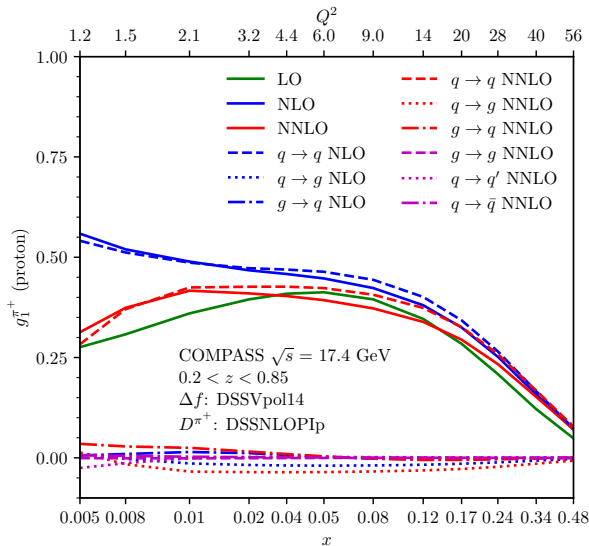


FIG. 2. Channel decomposition of theory predictions for $g_1^{\pi^+}$ with COMPASS kinematics.

To study the perturbative convergence of the polarized SIDIS predictions at higher energies, Fig. 3 displays $g_1^{\pi^+}$ (integrated over $0.2 < z < 0.85$) of the proton for EIC-like kinematics with $\sqrt{s} = 45$ GeV. We consider several values of Q^2 , and for each value of Q^2 we plot predictions for values of x constrained by the requirement $0.5 < y < 0.9$. Using the MAPPDF1.0 [38] and MAPFF1.0 [67] for polarized PDFs and FFs at NNLO throughout allows us to assess the uncertainty on the theory predictions in a consistent manner through a seven-point scale variation on μ_R and $\mu_F = \mu_A$, discarding extreme variations of one pair of scales.

For most of the range in x , we observe perturbative convergence of the predictions: while the LO/NLO ratio is of order 10–30%, we note that in the range $0.005 < x < 0.5$ the NNLO/NLO ratio is approximately 5%, slightly increasing towards smaller or larger values of x . Even though the size of the NNLO and NLO uncertainties are comparable at the level of about $\pm 8\%$, we however notice a slight reduction of the uncertainty envelope at NNLO for large values of x and Q^2 .

CONCLUSIONS

Important information on the quark flavor decomposition of the proton spin content is gained from polarization asymmetries in SIDIS. We computed the NNLO QCD corrections to the polarized SIDIS coefficient functions, which turn out to have a sizable numerical impact on the asymmetries especially at low x and low Q^2 . Our results allow to include polarized SIDIS data in future NNLO precision studies of polarized parton distributions,

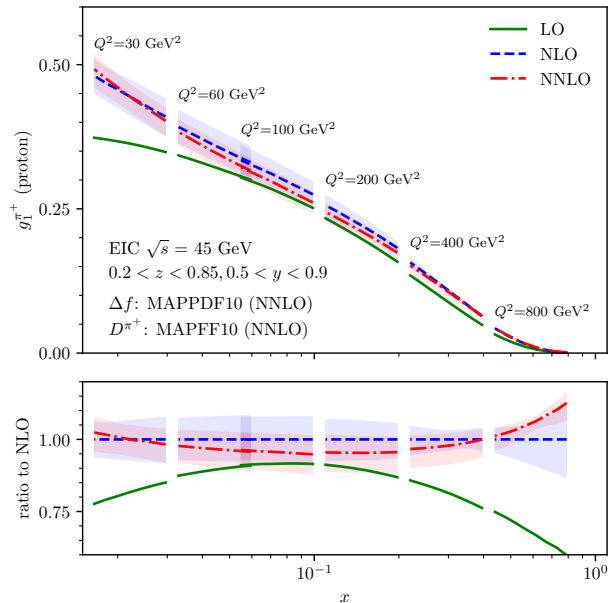


FIG. 3. Longitudinally polarized SIDIS structure function $g_1^{\pi^+}$ for EIC kinematics at $\sqrt{s} = 45$ GeV, evaluated at different perturbative orders.

thereby enabling an unprecedented level of detail in the understanding of the spin structure of the proton.

Acknowledgments.—We are grateful to Daniel de Florian for providing us with the DSSV PDF sets, and to Valerio Bertone, Amedeo Chiefa and Emanuele Nocera for discussions. This work has received funding from the Swiss National Science Foundation (SNF) under contract 200020-204200 and from the European Research Council (ERC) under the European Union’s Horizon 2020 research and innovation program grant agreement 101019620 (ERC Advanced Grant TOPUP).

- [1] J. Gao, L. Harland-Lang, and J. Rojo, *Phys. Rept.* **742**, 1 (2018), arXiv:1709.04922 [hep-ph].
- [2] S. Bailey, T. Cridge, L. A. Harland-Lang, A. D. Martin, and R. S. Thorne, *Eur. Phys. J. C* **81**, 341 (2021), arXiv:2012.04684 [hep-ph].
- [3] T.-J. Hou *et al.*, *Phys. Rev. D* **103**, 014013 (2021), arXiv:1912.10053 [hep-ph].
- [4] R. D. Ball *et al.* (NNPDF), *Eur. Phys. J. C* **82**, 428 (2022), arXiv:2109.02653 [hep-ph].
- [5] C. A. Aidala, S. D. Bass, D. Hasch, and G. K. Mallot, *Rev. Mod. Phys.* **85**, 655 (2013), arXiv:1209.2803 [hep-ph].
- [6] A. Accardi *et al.*, *Eur. Phys. J. A* **52**, 268 (2016), arXiv:1212.1701 [nucl-ex].
- [7] E. R. Nocera, R. D. Ball, S. Forte, G. Ridolfi, and J. Rojo (NNPDF), *Nucl. Phys. B* **887**, 276 (2014), arXiv:1406.5539 [hep-ph].

- [8] D. de Florian, R. Sassot, M. Stratmann, and W. Vogelsang, Phys. Rev. Lett. **113**, 012001 (2014), arXiv:1404.4293 [hep-ph].
- [9] J. Ashman *et al.* (EMC), Nucl. Phys. B **328**, 1 (1989).
- [10] B. Adeva *et al.* (SMC), Phys. Rev. D **58**, 112001 (1998).
- [11] P. L. Anthony *et al.* (E142), Phys. Rev. D **54**, 6620 (1996), arXiv:hep-ex/9610007.
- [12] K. Abe *et al.* (E143), Phys. Rev. D **58**, 112003 (1998), arXiv:hep-ph/9802357.
- [13] K. Abe *et al.* (E154), Phys. Rev. Lett. **79**, 26 (1997), arXiv:hep-ex/9705012.
- [14] P. L. Anthony *et al.* (E155), Phys. Lett. B **493**, 19 (2000), arXiv:hep-ph/0007248.
- [15] A. Airapetian *et al.* (HERMES), Phys. Rev. D **75**, 012007 (2007), arXiv:hep-ex/0609039.
- [16] C. Adolph *et al.* (COMPASS), Phys. Lett. B **753**, 18 (2016), arXiv:1503.08935 [hep-ex].
- [17] B. Adeva *et al.* (SMC), Phys. Lett. B **420**, 180 (1998), arXiv:hep-ex/9711008.
- [18] M. G. Alekseev *et al.* (COMPASS), Phys. Lett. B **693**, 227 (2010), arXiv:1007.4061 [hep-ex].
- [19] A. Airapetian *et al.* (HERMES), Phys. Rev. D **99**, 112001 (2019), arXiv:1810.07054 [hep-ex].
- [20] R. Abdul Khalek *et al.*, Nucl. Phys. A **1026**, 122447 (2022), arXiv:2103.05419 [physics.ins-det].
- [21] E. C. Aschenauer, I. Borsa, R. Sassot, and C. Van Hulse, Phys. Rev. D **99**, 094004 (2019), arXiv:1902.10663 [hep-ph].
- [22] W. Vogelsang, Nucl. Phys. B **475**, 47 (1996), arXiv:hep-ph/9603366.
- [23] R. Mertig and W. L. van Neerven, Z. Phys. C **70**, 637 (1996), arXiv:hep-ph/9506451.
- [24] S. Moch, J. A. M. Vermaseren, and A. Vogt, Nucl. Phys. B **889**, 351 (2014), arXiv:1409.5131 [hep-ph].
- [25] J. Blümlein, P. Marquard, C. Schneider, and K. Schönwald, Nucl. Phys. B **971**, 115542 (2021), arXiv:2107.06267 [hep-ph].
- [26] J. Blümlein, P. Marquard, C. Schneider, and K. Schönwald, JHEP **01**, 193 (2022), arXiv:2111.12401 [hep-ph].
- [27] E. B. Zijlstra and W. L. van Neerven, Nucl. Phys. B **417**, 61 (1994), [Errata: Nucl.Phys.B 426, 245 (1994); Nucl.Phys.B 773, 105–106 (2007); Nucl.Phys.B 501, 599–599 (1997)].
- [28] J. Blümlein, P. Marquard, C. Schneider, and K. Schönwald, JHEP **11**, 156 (2022), arXiv:2208.14325 [hep-ph].
- [29] D. de Florian, M. Stratmann, and W. Vogelsang, Phys. Rev. D **57**, 5811 (1998), arXiv:hep-ph/9711387.
- [30] M. Glück and E. Reya, Z. Phys. C **39**, 569 (1988).
- [31] G. Altarelli and W. J. Stirling, Part. World **1**, 40 (1989).
- [32] M. Glück, E. Reya, M. Stratmann, and W. Vogelsang, Phys. Rev. D **53**, 4775 (1996), arXiv:hep-ph/9508347.
- [33] T. Gehrmann and W. J. Stirling, Phys. Rev. D **53**, 6100 (1996), arXiv:hep-ph/9512406.
- [34] Y. Goto *et al.* (Asymmetry Analysis), Phys. Rev. D **62**, 034017 (2000), arXiv:hep-ph/0001046.
- [35] D. de Florian, R. Sassot, M. Stratmann, and W. Vogelsang, Phys. Rev. Lett. **101**, 072001 (2008), arXiv:0804.0422 [hep-ph].
- [36] D. de Florian, R. Sassot, M. Stratmann, and W. Vogelsang, Phys. Rev. D **80**, 034030 (2009), arXiv:0904.3821 [hep-ph].
- [37] J. Blümlein and H. Böttcher, Nucl. Phys. B **841**, 205 (2010), arXiv:1005.3113 [hep-ph].
- [38] V. Bertone, A. Chiefa, and E. R. Nocera, (2024), arXiv:2404.04712 [hep-ph].
- [39] M. Abele, D. de Florian, and W. Vogelsang, Phys. Rev. D **104**, 094046 (2021), arXiv:2109.00847 [hep-ph].
- [40] S. Goyal, S.-O. Moch, V. Pathak, N. Rana, and V. Ravindran, (2023), arXiv:2312.17711 [hep-ph].
- [41] L. Bonino, T. Gehrmann, and G. Stagnitto, (2024), arXiv:2401.16281 [hep-ph].
- [42] D. P. Anderle, F. Ringer, and W. Vogelsang, Phys. Rev. D **87**, 094021 (2013), arXiv:1304.1373 [hep-ph].
- [43] A. Airapetian *et al.* (HERMES), Phys. Rev. D **71**, 012003 (2005), arXiv:hep-ex/0407032.
- [44] D. Anderle, D. de Florian, and Y. Rotstein Habarnau, Phys. Rev. D **95**, 034027 (2017), arXiv:1612.01293 [hep-ph].
- [45] G. 't Hooft and M. J. G. Veltman, Nucl. Phys. B **44**, 189 (1972).
- [46] P. Breitenlohner and D. Maison, Commun. Math. Phys. **52**, 11 (1977).
- [47] S. A. Larin and J. A. M. Vermaseren, Phys. Lett. B **259**, 345 (1991).
- [48] S. A. Larin, Phys. Lett. B **303**, 113 (1993), arXiv:hep-ph/9302240.
- [49] K. G. Chetyrkin and F. V. Tkachov, Nucl. Phys. B **192**, 159 (1981).
- [50] S. Laporta, Int. J. Mod. Phys. A **15**, 5087 (2000), arXiv:hep-ph/0102033.
- [51] A. von Manteuffel and C. Studerus, (2012), arXiv:1201.4330 [hep-ph].
- [52] T. Gehrmann and E. Remiddi, Nucl. Phys. B **580**, 485 (2000), arXiv:hep-ph/9912329.
- [53] L. Bonino, T. Gehrmann, R. Schürmann, and G. Stagnitto, “Antenna subtraction for processes with identified particles at hadron colliders,” In preparation.
- [54] T. Gehrmann and R. Schürmann, SciPost Phys. Proc. **7**, 042 (2022), arXiv:2110.02617 [hep-ph].
- [55] T. Gehrmann, T. Huber, and D. Maitre, Phys. Lett. B **622**, 295 (2005), arXiv:hep-ph/0507061.
- [56] J. A. M. Vermaseren, (2000), arXiv:math-ph/0010025.
- [57] E. Remiddi and J. A. M. Vermaseren, Int. J. Mod. Phys. A **15**, 725 (2000), arXiv:hep-ph/9905237.
- [58] D. Maitre, Comput. Phys. Commun. **174**, 222 (2006), arXiv:hep-ph/0507152.
- [59] C. Duhr and F. Dulat, JHEP **08**, 135 (2019), arXiv:1904.07279 [hep-th].
- [60] S. L. Adler, Phys. Rev. **177**, 2426 (1969).
- [61] J. S. Bell and R. Jackiw, Nuovo Cim. A **60**, 47 (1969).
- [62] Y. Matiounine, J. Smith, and W. L. van Neerven, Phys. Rev. D **58**, 076002 (1998), arXiv:hep-ph/9803439.
- [63] M. Höschele, J. Hoff, A. Pak, M. Steinhauser, and T. Ueda, Comput. Phys. Commun. **185**, 528 (2014), arXiv:1307.6925 [hep-ph].
- [64] A. D. Martin, R. G. Roberts, W. J. Stirling, and R. S. Thorne, Eur. Phys. J. C **28**, 455 (2003), arXiv:hep-ph/0211080.
- [65] D. de Florian, R. Sassot, and M. Stratmann, Phys. Rev. D **75**, 114010 (2007), arXiv:hep-ph/0703242.
- [66] R. D. Ball *et al.* (NNPDF), Eur. Phys. J. C **77**, 663 (2017), arXiv:1706.00428 [hep-ph].
- [67] R. Abdul Khalek, V. Bertone, A. Khoudli, and E. R. Nocera, Phys. Lett. B **834**, 137456 (2022), arXiv:2204.10331 [hep-ph].